Quantitative studies of two-dimensional first- and second-order phase transitions by integrating diffraction methods

1999 J. Phys.: Condens. Matter 11 9933

(http://iopscience.iop.org/0953-8984/11/49/311)

J. Phys.: Condens. Matter **11** (1999) 9933–9942. Printed in the UK PII: S0953-8984(99)04930-9

Quantitative studies of two-dimensional first- and second-order phase transitions by integrating diffraction methods

H Pfnür†¶, C Voges†, K Budde†, I Lyuksyutov‡§ and H-U Everts‖

† Institut für Festkörperphysik, Universität Hannover, Appelstraße 2, D-30167 Hannover, Germany

‡ Department of Physics, Texas A& M University, College Station, TX 77843-4242, USA

§ Institute of Physics, Academy of Sciences of the Ukraine, Prospect Nauki 46, 252028 Kiev, Ukraine

‖ Institut für Theoretische Physik, Universität Hannover, Appelstraße 2, D-30167 Hannover, Germany

Received 2 June 1999

Abstract. Using low-energy electron diffraction (LEED), we show for two classes of systems, which are representative for second- and first-order phase transitions in adsorbed layers, that quantitative properties of phase transitions can be studied also by using integrated diffracted intensities, turning the instrument to low resolution in two-dimensional reciprocal space, $k_{\parallel}$. For the continuous order–disorder phase transitions of several atomic adsorption systems, critical properties have been studied by determination of the critical exponents α (of the specific heat) and η, the anomalous critical dimension, in the limit $k_{\parallel}\xi \gg 1$. We performed systematic tests of the conditions under which these exponents can be determined reliably from the diffracted intensity of superstructure beams. In first-order phase transitions, scaling laws characterize specific mechanisms driving the transitions. As an example of two-dimensional first-order phase transitions, the transitions between a two-dimensional (2D) gas and the 2D solid of the first monolayer have been studied for the noble gases Ar, Kr and Xe on a NaCl(100) surface in quasi-equilibrium with the three-dimensional (3D) gas phase. Using linear temperature ramps, we show that the widths of the hysteresis loops of these transitions as a function of the heating rate, r, scale with a power law $\propto r^x$ with x between 0.4 and 0.5 depending on the system. The hysteresis loops for different heating rates are similar. The island area of the condensed layer was found to grow initially with a time dependence $\propto t^4$. These results are in agreement with a model of growth-controlled hysteresis, which predicts $x = 0.5$ and hysteresis loop similarity.

1. Introduction

Phase transitions are generally driven by fluctuations, which can be characterized by their correlation lengths, ξ. For first-order transitions, the correlation length remains finite. Close to the transition the coexisting phases can easily be overheated and undercooled, leading to the well-known hysteresis phenomena. These depend partly on boundary conditions such as heterogeneous or homogeneous nucleation, but even more strongly on the processes controlling the dynamics of transformation from one phase into the other. Thus detailed studies of the dynamics of first-order phase transitions contain information about the mechanism driving the phase transition.

¶ Author to whom any correspondence should be addressed.

0953-8984/99/499933+10$30.00

For continuous phase transitions on the other hand, the correlation length in an ideal system should diverge at the critical point. Therefore, their quantitative properties should only depend on dimension and on the change of symmetry at the phase transition. This picture has been corroborated both theoretically [1–3] and to some extent experimentally [4] also for two-dimensional systems. Due to the much larger influence of fluctuations in 2D compared to three-dimensional systems, large deviations from mean-field behaviour are expected and have been observed in several different universality classes [1, 2]. In our own experience, strongly chemisorbed atomic adsorbates at concentrations of sub-monolayers on metal surfaces represent very good model systems for such studies [5, 6]. Their continuous order–disorder phase transitions of commensurate phases give access to a variety of different universality classes in 2D, which would mostly not be accessible via magnetic systems.

In this paper, we concentrate on examples of scaling laws for first- and second-order phase transitions, which can be explored by use of integrated LEED intensities. For continuous phase transitions, we performed tests on three systems with two different symmetries, namely on (2×2)-ordered H/Ni(111) and S/Ru(0001), and on $(\sqrt{3} \times \sqrt{3})$R30°-ordered S/Ru(0001). In particular, the system H/Ni(111) represents a crucial test system due to its small scattering amplitude. The order–disorder phase transitions of the (2×2) phases on both surfaces have been shown to indeed be continuous and to belong to the four-state Potts universality class [7,8], whereas the transition of the $\sqrt{3} \times \sqrt{3}$R30° structure belongs to the three-state Potts class [7].

As examples of first-order phase transitions, we investigated in our experiments the scaling of the hysteresis loops during condensation of the 2D solid phases of the noble gases Xe, Kr and Ar on single-crystalline thin films of NaCl(100) in quasi-equilibrium with the 3D gas phase at room temperature. Due to the van der Waals attraction between the noble-gas atoms, these transitions are strongly first order, and can easily be measured. Since these gases condense in different 2D structures (quasi-hexagonal (Xe) and quadratic (Ar, Kr)), our experiments demonstrate that hysteresis loop scaling does not depend on the details of the solidification process.

Most of the current experiments on two-dimensional systems trying to test hysteresis loop scaling have been carried out on ferromagnetic layers [9–11]. Their objective has been to check the validity of the scaling law [12, 13]

$$\mathcal{A} \propto H_0^x \Omega^y \tag{1}$$

for the area $\mathcal{A}$, i.e. the energy loss per cycle, of the hysteresis loop induced by a sinusoidal magnetic field $H(t) = H_0 \sin \Omega t$.

However, the underlying physical mechanisms are far from being understood: although power-law behaviour has been found in all studies [9–11], corroborating the general concept expressed by equation (1), the effective exponents x, y obtained from measurements on magnetically quite similar systems vary by up to one order of magnitude (for a more detailed discussion, see reference [11]).

In this situation, it seemed to be highly desirable to explore the validity of hysteresis loop scaling in a completely different physical context: the condensation of the first layer of an adsorbate on a surface with the heat of adsorption as the latent heat is a typical first-order process for 2D systems (see [14]), which exhibits in many cases hysteresis due to overheating and undercooling of the overlayer in an adsorption–desorption cycle [15]. In adsorption the deviation μ of the chemical potential from its equilibrium value at the phase transition plays the role of the magnetic field. Correspondingly, H_0 must be replaced by the amplitude of the varying chemical potential, μ_0, in equation (1). Both the dynamics of magnetization reversal in thin films and that of solidification of 2D adsorbed layers are governed by domain wall dynamics, i.e. by domain nucleation and domain growth. The important difference between

magnetic films and 2D adsorption layers is that in magnetic films the domain wall width is typically of the order of 20 nm, whereas the boundaries of adsorbate islands, which play the role of domain walls in adsorption dynamics, are sharp on the atomic scale. As a consequence, nucleation barriers and hence the nucleation time τ_n can be much smaller in adsorbed layers than in magnetic films.

The studies of continuous phase transitions have a very different aim. Here, fluctuations occur on all length scales, so an instrument which integrates effectively over all long-range correlations will also be able to measure critical properties. In the limit where the integration radius, k_I, around a superstructure beam fulfils the condition $k_I\xi \gg 1$, these averages are predicted to have the same critical properties as the *energy* [16], i.e. they should diverge at the critical point as a function of reduced temperature t ($t = (T - T_c)/T_c$) with $t^{1-\alpha}$. (T_c is the critical temperature.) There have been successful experiments which directly measured the specific heat for noble-gas monolayers on graphite [17, 18]. They were able to identify α for both the Ising [17] and the three-state Potts universality classes [18]. However, this type of experiment is impossible for single crystals because of their small surface-to-volume ratio. Therefore, the method just described is the only possibility. There have been some attempts both in experiments [7, 19, 20] and in simulations [21] to prove the energy-like behaviour in scattering experiments for order–disorder phase transitions in two-dimensional layers. However, the results were all more or less inconclusive, since none of them showed pure power-law behaviour; instead they showed rather large deviations from the expected exponents of known universality classes. If the determination of α worked reliably under well-defined conditions, is would provide an easy experimental test of the nature of a given phase transition, and an easy discrimination between various universality classes, since the differences in α between different universality classes are the largest among the various critical exponents. Systematic tests are necessary, therefore.

Using integrated LEED intensities, the critical exponent η, the anomalous critical dimension, can also be determined, since in the limit $k_\parallel\xi \to \infty$ critical scattering has a leading term [22]

$$\chi(k_\parallel, t) = C\xi^{\gamma/\nu} D_\pm = k_\parallel^{-(2-\eta)}(1 + \cdots) \tag{2}$$

which is independent of temperature. If this limit can be reached experimentally, η can be determined by integrating the intensity in a ring around a superstructure spot:

$$R_I = 2\pi \int_{k_1}^{k_2} k \, \mathrm{d}k \, I(k) \approx A_\pm \frac{\pi}{1-\eta}(k_2^\eta - k_1^\eta) \tag{3}$$

thereby avoiding any contribution from long-range order, which is centred at the Bragg position.

By systematic variation of the radii of integration around two-dimensional superstructure Bragg positions, it turns out that the limit $k_\parallel\xi \gg 1$ can be reached rather easily, so the critical exponents α and η can be determined reliably by integrating methods with LEED.

2. Experimental procedure

All of the experiments were carried out in μ-metal-shielded UHV chambers (base pressure 2×10^{-11} mbar) pumped by titanium sublimation and turbo-molecular pumps. The equipment was supplemented by Auger and quadrupole mass spectrometers. LEED intensities were measured using a conventional back-view LEED optics or a high-resolution LEED optics equipped with a high-resolution optical detector. Peak intensities of LEED diffraction spots were measured both with a Faraday cup and with the optical detector, while integrated intensities were obtained from images taken with a cooled slow-scan CCD camera (512×512

pixels with 14-bit resolution) that were stored on a personal computer. The variation of the integration radii, background subtraction etc was carried out afterwards on the digitized images. The temperature of the samples, which were cooled either by liquid N_2 or by liquid He and heated resistively, radiatively or by electron bombardment, was controlled by thermocouples (Ni/NiCr or WRe 5%–WRe 25%) attached to a sample or in its close vicinity (NaCl). A computerized feedback circuit with a nominal resolution of 0.001 K stabilized the sample temperature to ± 0.01 K. The samples (10 mm in diameter, 1.5 mm thick) were cut by spark erosion from single-crystal rods, etched, precision oriented to better than 0.2° and polished with diamond pastes down to 0.25 μm grain size. After extensive sputtering/annealing cycles had been carried out for Ni (heating/cooling cycles in 5×10^{-7} mbar oxygen for Ru), no contaminants were detectable any longer with Auger spectroscopy long before these cycles were completed. The NaCl(100) surfaces were prepared *in situ* as epitaxial films three double layers thick by evaporation of NaCl onto a Ge(100) substrate at a surface temperature of 200 K and subsequently annealed to 550 K. This procedure produces single-crystalline NaCl layers of high quality [23].

The temperature ramps for hysteresis measurements were always started far outside the range of the phase transitions, so stable linear ramps with deviations close to the resolution of the temperature control were obtained in all cases.

For Xe on NaCl(100), the superstructure diffraction spots of the quasi-hexagonal incommensurate structure [24] were directly used to measure the hysteresis both with integrated and with peak intensities. Only peak intensities of integer-order beams were evaluated for the monolayers of Ar and Kr, which form ordered (1×1) and diffuse (2×1) structures, respectively.

3. Results and discussion

3.1. First-order transitions: testing of dynamical scaling

The physical scenario that we want to test by means of our experiments on hysteresis loop scaling has been outlined recently [25]. It makes the following assumption: hysteresis loop scaling is studied close to thermodynamical equilibrium, so that it is controlled close to the phase transition to condensation by the deviation of the chemical potential, μ, from its value at infinitely slow approach to the phase transition, μ_0. It further assumes heterogeneous nucleation, which does not limit the speed of condensation, and a speed of island growth, v, with $v \propto \mu$. With these assumptions, which we call growth-controlled hysteresis, it can easily be shown [25, 26] that for linear heating rates:

(a) the area of the hysteresis loop, $\mathcal{A}$, scales with the heating rate, r, as r^x with $x = 0.5$;
(b) during the initial stage of growth, the coverage of the condensate grows with time as t^4;
(c) hysteresis loops are self-similar.

These results of the model can easily be tested in our experiments, in which we linearly ramp the surface temperature up and down, keeping the ambient gas pressure constant. Since the integrated intensity of a superstructure spot, I, in a diffraction experiment is proportional to the coverage, Θ, statement (b) can be tested easily by measuring the initial time dependence of I.

Typical data on the hysteresis during condensation of the quasi-hexagonal Xe layer are shown in figure 1. The linear heating rate was varied by two orders of magnitude between 0.001 and 0.1 K s^{-1}. This rate was limited at small rates by the resolution of the temperature measurement, at high rates by the onset of intermixing of second-layer

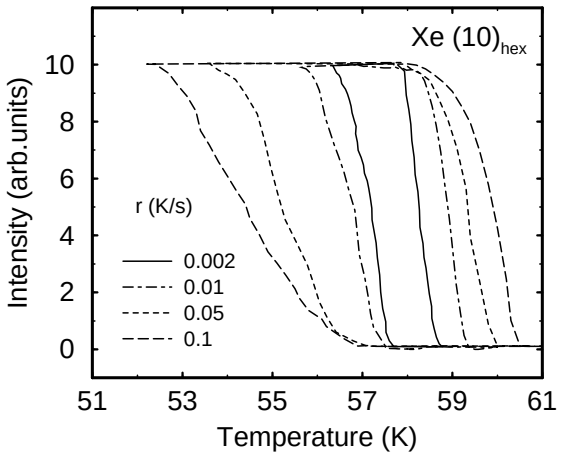

Figure 1. Hysteresis loops of the 2D gas–solid phase transition of Xe/NaCl(100) at a Xe pressure of 10^{-7} mbar. The intensity of a first-order superstructure spot was monitored at the heating rates indicated.

condensation. Measurements were taken for gas pressures of 10^{-6} and 10^{-7} mbar. Not surprisingly, the slopes during adsorption and desorption are not symmetrical due to the exponential dependence of the desorption rate on the surface temperature. At higher rates the form during condensation changes due to the above-mentioned onset of intermixing with second-layer adsorption, leading also to a decrease of intensity with decreasing temperature. Inside these limits the intensity at saturation did not depend on the heating rate.

For all three systems, we evaluated the dependence of the widths of the hysteresis loops at half-maximum intensity on the heating rate r. The results are shown as log–log plots in figure 2. Power laws with similar effective exponents were obtained for all three systems, although the shapes of the hysteresis loops differ significantly from each other. The effective exponents α obtained from these plots are close to 0.4 for Xe and Ar condensation (within the statistical uncertainty of about 10%), whereas the average value for Kr of $\alpha = 0.50$ actually corresponds exactly to the value expected from the simple model of growth-controlled hysteresis already mentioned. This perfect agreement might be accidental. The roughly 20% smaller values obtained for Xe and Ar are sufficiently close to $\alpha = 0.5$ to exclude a change of

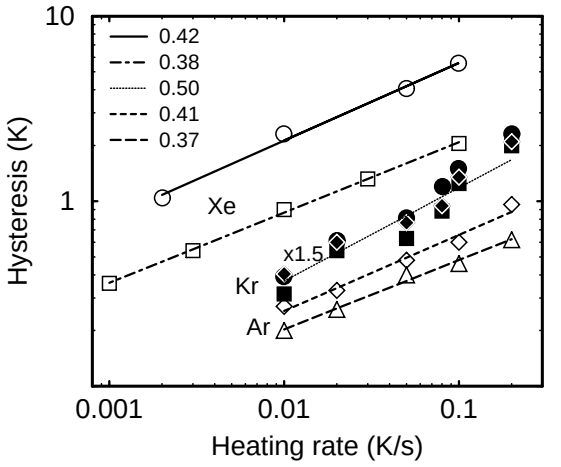

Figure 2. Log–log plots of the widths of hysteresis loops as functions of the heating rate r in the presence of a 3D gas pressure. Xe/NaCl(100): $p = 1 \times 10^{-7}$ mbar (◯), $p = 1 \times 10^{-6}$ mbar (□). Full symbols: Kr/NaCl(100) at $p = 1 \times 10^{-7}$ mbar (three different orders of diffraction). ◇ and △: Ar/Nacl(100) at $p = 1 \times 10^{-7}$ mbar measured for the (10) and (11) beams, respectively.

the basic condensation mechanism to nucleation-controlled growth, but these deviations might nevertheless lead us to question the validity of our simple model.

Therefore, we also tested the time dependence of island growth during the initial stages of growth for Xe. For this purpose, we plotted the integrated intensities of the Xe system as a function of time during condensation again on a log–log scale (see figure 3). As mentioned, the model predicts the integrated intensity to increase $\propto r^2 t^4$. Since the temperature deviation from the equilibrium condensation point is $\Delta T = rt$, the integrated intensity should grow $\propto (\Delta T)^4/r^2$. Therefore, the data in this figure are plotted once as a function of ΔT, and a second time scaled by r^{-2}. The integrated intensities follow closely the t^4-dependence predicted by our simple model, but deviate for coverages close to saturation, as expected. As time zero we chose the condensation temperature at equilibrium, as estimated from the centre of the hysteresis curves. This is the earliest possible time. It is fully consistent with the assumptions of the model used, which assumes a small nucleation time τ_n. The intensity zero was taken as the bottom of the hysteresis curves without further adjustments. This result therefore seems to nicely corroborate the model assumptions of growth-controlled hysteresis and of a linear dependence of island growth on the deviation of the chemical potential from the equilibrium value.

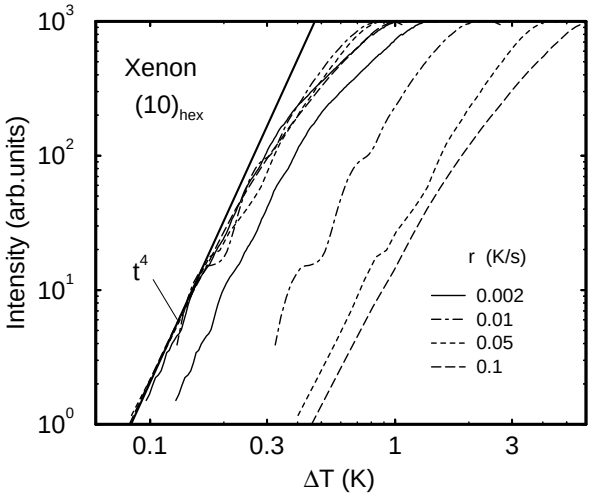

Figure 3. Testing of the scaling with time of integral intensities of a first-order superstructure spot of Xe/NaCl(100). The four data sets for the heating rates indicated are also shown after rescaling by r^{-2} (leftmost sets) together with a t^4-line.

These results turned out to be insensitive to additional production of anion vacancies on the NaCl substrate, caused by the measuring electron beam. They act as additional nucleation centres. Though they reduce the maximum size of the islands, they obviously do not change the growth modes, in agreement with the expectations from our model.

An explicit test of the similarity of the hysteresis curves was again carried out for Xe/NaCl(100). The rescaled curves (after centring) are shown in figure 4 for one-order-of-magnitude changes in the heating rate. While the evaporation data fit perfectly to a common line, there is more scatter in the data during condensation, but no general trend for the small deviations was found. Therefore, similarity also seems to be fulfilled by these data.

These results and their close agreement with theoretical expectations based on a simple model shows that our approach allows access to a variety of scenarios of first-order processes in two-dimensional systems and to two-dimensional interface motion. The good agreement between our model and the experiments is in sharp contrast with the situation in magnetic films where large discrepancies between experiment and theory have occurred. Possible reasons for the more favourable situation in adsorption are the small widths of the island boundaries (of the

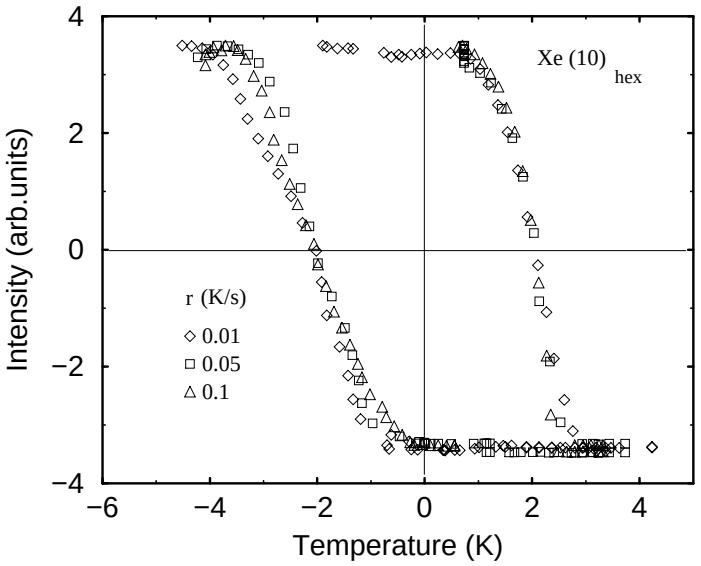

Figure 4. Hysteresis curves for Xe rescaled by $(\Delta T)^{-\alpha}$.

order of one lattice constant) and/or a low interface energy. Both features would lead to small nucleation barriers and hence to short nucleation times. This is consistent with the observation that growth-controlled hysteresis is the dominant mechanism in our experiments.

3.2. Continuous phase transitions: determination of the critical exponents α and η

As mentioned in the introduction, we tested in these experiments the feasibility of reliably determining the critical exponents α and η from integrated intensities of superstructure beams. More details of these investigations can be found in reference [27].

First, the thermal diffuse background that has to be subtracted from the integral intensities was measured at $k_{\|}$-positions exactly between the superstructure spots and averaged over a diameter of 12% of $|k_{10}|$ in the temperature range $\pm 10\%$ around the phase transitions. No further adjustments of the resulting integral intensities were made.

T_c was determined from the point of inflection of the integrated curves [16], i.e. from the peak of the temperature derivatives of the integrated intensities, I'. (H/Ni(111)-p(2 × 2): $T_c = 268.2$ K, S/Ru(0001)-p(2 × 2): $T_c = 471.1$ K, S/Ru(0001)-($\sqrt{3} \times \sqrt{3}$)R30°: $T_c = 416.0$ K.) The accuracy of T_c of ± 0.5 K turned out to be the main source of uncertainty in the determination of α. With T_c fixed as described, effective values of α were obtained from log–log plots of I' for various integration radii, k_I. As a typical example, the left panel of figure 5 shows I' for the (2 × 2) systems H/Ni(111) and S/Ru(0001) below T_c. Below T_c, a power-law behaviour is seen over slightly less than one order of magnitude in t between 0.01 and 0.1 for H/Ni(111), almost independently of the integration radius, which was varied between 0.6% and 4% of the Brillouin zone (BZ) diameter. Whereas the lower limit of the integration radius is due to the finite resolution of the LEED instrument, the variation of I' (as a function of k_I) for integration radii larger than 4% was found to be small. With the much higher signal in the system S/Ru(0001)-p(2 × 2), no deviations from power-law behaviour at large t are seen and practically identical values for α were obtained ($\alpha = 0.68 \pm 0.07$ H/Ni(111) and 0.66 ± 0.07 for S/Ru(0001)). They coincide almost perfectly with those of the expected four-state Potts universality class. The levelling off at $|t| < 0.01$ is due to the finite

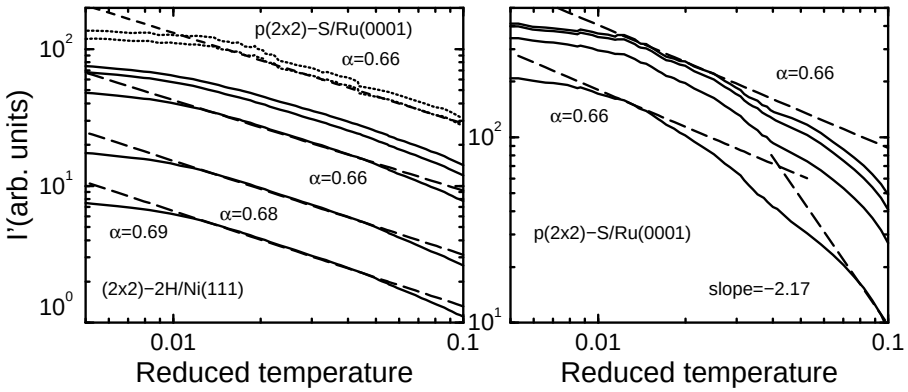

Figure 5. Log–log plots of integrated intensities of superstructure beams as functions of reduced temperature for (2 × 2)-2H/Ni(111) and p(2 × 2) S/Ru(0001) below T_c (left), and for p(2 × 2) S/Ru(0001) above T_c, for various radii of integration. In the left panel, these radii vary between 0.6% (lowest curve) and 4% (in units of $|k_{10}|$) for H/Ni(111). For S/Ru(0001), the curves for radii of $k_I = 2.7$ and 4% (short dashes) are shown. In the right panel the variation is between 1.35% and 8%.

size of the terraces on our surfaces. The deviations from power-law behaviour close to $t = 0.1$ for H/Ni(111) might be an experimental effect due to incorrect background subtraction, since these deviations were not seen for S/Ru(0001). A comparison of previously measured data for the correlation lengths at these phase transitions [7,8] shows that the crossover to the finite-size regime happens roughly when the correlation length reaches the average terrace size.

Similar behaviour in the same range of t is observed for I' on the $(\sqrt{3} \times \sqrt{3})$R30°-S/Ru(0001), but with an effective exponent α of 0.40 ± 0.05. This value is slightly larger than expected for the three-state Potts universality class ($\alpha = 1/3$), but any attempt to add additional terms to the simple power law only made the value of α more dependent on the integration radius, and did not systematically shift it closer to $1/3$. The most likely explanation for this discrepancy is the small influences of the crossover to the behaviour at small $k_\parallel \xi$ with an exponent $(1 - 2\beta)$, which is 0.78 and 0.83, respectively, for three- and four-state Potts classes. Since α is much closer to $1 - 2\beta$ for the four-state Potts systems than for the three-state Potts system, this effect is much more severe in the latter case, in agreement with our observation, and is a likely explanation for our findings.

Above T_c, apart from the finite-size-limited region in t, no power-law behaviour can be observed. As expected from qualitative calculations using an expansion in $4 - \epsilon$ dimensions [27], the accessible range of reduced temperature is completely dominated by crossover between $t^{-\alpha}$-behaviour and $t^{-\gamma-1}$-behaviour. This slope should be reached at large t, i.e. for very broad spots, where $k_I \xi \gg 1$ is no longer valid. Indeed, the limiting slope in the lowest curve of figure 5 (right panel) at large t corresponds exactly to this value. Putting the values for α obtained below T_c into this figure, a widening of the t-range can be recognized, as a function of increasing k_I, over which the slope α fits the curves. This range, however, is too small in all cases for α to be determined directly. On the other hand, using the known values of α and the correlation lengths determined from spot profile analysis as a function of t [7,8], we can estimate the limiting values of $k_\parallel \xi$ for the 'correct' slope of α to be between 1 and 2 for the (2 × 2) systems and around 3 for the $\sqrt{3}$ system. From the successful determination of α in the same t-range below T_c, and with similar k_I, we conclude that the limit of large $k_\parallel \xi$ is reached even more easily below T_c, although the correlation lengths for identical $|t|$ below T_c

are considerably smaller than above T_c [28].

From these results, we have good evidence that α can be determined reliably from integrated intensities, at least below T_c. Although corrections are non-universal and may play a role in all systems of finite size [3], they have been shown to have little influence in the determination of the exponents β, γ and ν [7, 8, 19] for the systems investigated here. Our results suggest that on these rather imperfect surfaces the most important modification of the effective values obtained for α seems to be crossover to $(1-2\beta)$ below T_c and to $(1+\gamma)$ above T_c. Below T_c, α is only slightly influenced but not dominated by crossover to $(1-2\beta)$. This effect should be strongly reduced closer to T_c, for which, however, surfaces with much larger terraces are needed.

In order to test equation (3), we integrated ring intensities around superstructure spots excluding the centre. Thus, the intensity due to long-range order did not contribute. A background subtraction as described above was carried out before analysing the data, which, as mentioned, contained no adjustable parameters. The circle at 4% of $|k_{10}|$ was arbitrarily chosen as zero. Figure 6 shows our results for $(\sqrt{3}\times\sqrt{3})$R30°-ordered S/Ru(0001) and for (2×2)-ordered H/Ni(111). Both data sets show the same trends: there is significant temperature dependence below $k_\parallel = 3\%$, but the integrated ring intensities above $k_\parallel = 4\%$ show little, but no systematic dependence on temperature, as predicted by equation (3). This is especially remarkable for the H/Ni(111) data, which go through the phase transition. The same behaviour, even up to an integration radius of 14%, was found for p(2×2)-S/Ru(0001). Fits to the data according to equation (3) were carried out for integration radii between 3 and 14% of $|k_{10}|$ for $(\sqrt{3}\times\sqrt{3})$R30°-S/Ru(0001). They yield an average value for $\eta = 0.30 \pm 0.08$. The same procedure applied to H/Ni(111) gives $\eta = 0.27 \pm 0.10$. The error limits contain variations of η from different data sets and uncertainties in background subtraction, which are more severe for the H/Ni(111) system due to the small absolute intensities in this system.

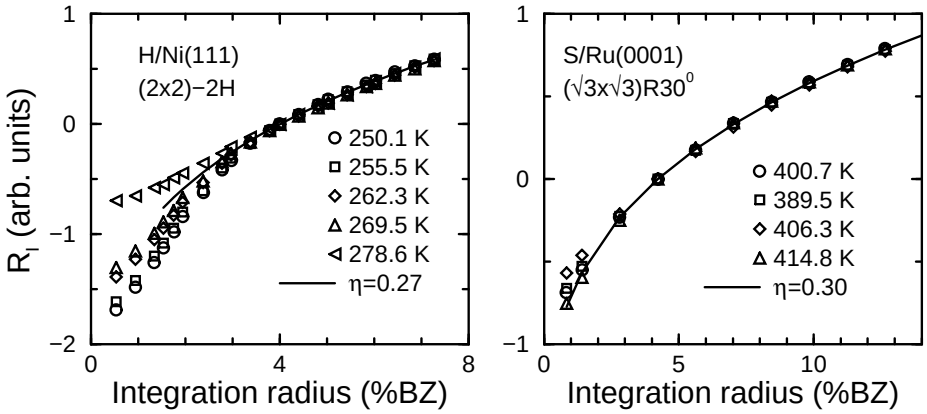

Figure 6. Integrated ring intensities, R_I, as functions of the integration radius $\Delta k_\parallel$, measured in units of the diameter of the Brillouin zone, BZ ($\equiv|k_{10}|$), at the temperatures indicated. Note that for H/Ni(111) T_c was at 268.2 K, i.e. data were taken both below and above T_c. The lower boundary in the integration was arbitrarily set to $\Delta k_\parallel = 0.04 k_{10}$.

Both values agree within error bars very well with those expected from theory ($\eta = 0.27$ for three-state Potts systems and 0.25 for four-state Potts systems), although obtained over a comparatively small range in $k_\parallel$. This range, however, cannot be extended both for physical reasons (the boundary of the Brillouin zone) and for reasons of too-small intensities.

These experiments demonstrate that at continuous order–disorder phase transitions in two-dimensional lattice gas systems belonging to the three- and four-state Potts universality classes, the limit of large $k_\parallel\xi$ is reached above T_c already for values of $k_\parallel\xi$ between 2 and 3, whereas below T_c these values are even smaller. As a consequence, the successful determination of the critical exponent of the specific heat, α, is possible below T_c even rather far away from the critical temperature, but (small) crossover effects to behaviour $\propto(2\beta - 1)$ are detectable.

The feasibility of reaching the limit of large $k_\parallel\xi$ rather easily in experiment has the interesting consequence that we can demonstrate that critical scattering in this limit is dominated by a term which is independent of temperature. By explicit determination of η we also show that the $k_\parallel$-dependence is fully compatible with that given by equation (2).

Acknowledgments

We wish to thank V L Pokrovsky for extensive discussions on the problem of hysteresis loop scaling. The work was supported by the MWK of Niedersachsen, by VW Stiftung and by the Deutsche Forschungsgemeinschaft. One of us (IL) was partly supported by a DOE grant (DE-FG03-96ER 45598).

References

[1] Persson B N J 1992 *Surf. Sci. Rep.* **15** 1
[2] Einstein T L 1988 *Chemistry and Physics of Solid Surfaces VII* ed R Vanselow and R Howe (Heidelberg: Springer) p 307
[3] Shalaev B 1994 *Phys. Rep.* **237** 129
[4] Bauer E 1987 *Springer Topics in Current Physics* vol 43 (Heidelberg: Springer) p 115
[5] Piercy P and Pfnür H 1987 *Phys. Rev. Lett.* **59** 1124
[6] Nakajima Y, Voges C, Nagao T, Hasegawa S and Pfnür H 1997 *Phys. Rev.* B **55** 8129
[7] Sokolowski M and Pfnür H 1994 *Phys. Rev.* B **49** 7716
[8] Budde K, Schwenger L, Voges C and Pfnür H 1995 *Phys. Rev.* B **52** 9275
[9] He Y-L and Wang G-C 1993 *Phys. Rev. Lett.* **70** 2336
[10] Jiang Q, Yang H-N and Wang G-C 1995 *Phys. Rev.* B **52** 14 911
[11] Suen J-S and Erskine J L 1997 *Phys. Rev. Lett.* **78** 3567
[12] Rao M, Krishnamurty H R and Pandit R 1990 *Phys. Rev.* B **42** 856
[13] References to theoretical work can be found in [11].
[14] Zangwill A 1988 *Physics at Surfaces* (Cambridge: Cambridge University Press)
[15] Bruch L W, Cole M W and Zaremba E 1997 *Physical Adsorption: Forces and Phenomena* (Oxford: Clarendon)
[16] Bartelt N C, Einstein T L and Roelofs L D 1985 *Phys. Rev.* B **32** 2993
[17] Tejwani M O, Ferreira O and Vilches O E 1980 *Phys. Rev. Lett.* **44** 152
[18] Bretz M 1977 *Phys. Rev. Lett.* **38** 501
[19] Pfnür H and Piercy P 1989 *Phys. Rev.* B **40** 2515
[20] Unertl W N 1986 *Comment. Condens. Matter Phys.* **12** 289
[21] Bartelt N C, Einstein T L and Roelofs L D 1985 *Surf. Sci.* **149** L47
[22] Fisher M E 1974 *Rev. Mod. Phys.* **46** 597
[23] Schwennicke C, Schimmelpfennig J and Pfnür H 1993 *Surf. Sci.* **293** 57
[24] Schwennicke C, Schimmelpfennig J and Pfnür H 1993 *Phys. Rev.* B **48** 8928
[25] Lyuksyutov I F, Pfnür H and Everts H-U 1998 *Europhys. Lett.* **41** 395
[26] Budde K, Lyuksyutov I, Pfnür H, Godzik G and Everts H-U 1999 *Europhys. Lett.* **47** 575
[27] Voges C and Pfnür H 1998 *Phys. Rev.* B **57** 3345
[28] Bartelt N C, Einstein T L and Roelofs L D 1987 *Phys. Rev.* B **35** 1776